Study of Phonon Dispersion of Iridium Oxide $Ca_5Ir_3O_{12}$ with Strong Spin-orbit Interaction

Hiroki Hanate[1]* , Takumi Hasegawa[2], Satoshi Tsutsui[3], Kazuma Nakamura[1], Yoshihide Yoshimoto[4], Naohiro Kishigami[1], Sho Haneta[1] and Kazuyuki Matsuhira[1]†

[1] *Graduate School of Engineering, Kyushu Institute of Technology, Kitakyushu 804-8550, Japan*

[2] *Graduate School of Integrated Arts and Sciences, Hiroshima University, 1-7-1 Kagamiyama, Higashi-Hiroshima 739-8521, Japan*

[3] *Japan Synchrotron Radiation Research Institute (JASRI), SPring-8, Sayo, Hyogo 679-5198, Japan*

[4] *Graduate School of Information Science and Technology, University of Tokyo, Tokyo 113-0033, Japan*

In this study, we report the results of experiments and calculations of phonon dispersion of iridium oxide with a strong spin-orbit interaction (SOI). Using inelastic X-ray scattering (IXS), we measured the IXS spectra of $Ca_5Ir_3O_{12}$ along Γ-A, Γ-M, and Γ-K-M directions in the Brillouin zone of a hexagonal lattice at room temperature. We also show *ab initio* density-functional phonon dispersions based on local density approximation and generalized gradient approximation (GGA) considering SOI. By comparing the experimental and calculated results, we found that the GGA phonon dispersion with SOI is in very good agreement with the experimental results. The phonon calculation was performed for supercells of 1×1×3 and preliminary 2×2×1. We found no phonon instability within these supercells. Low-energy phonon properties such as Debye temperature, specific heat, and sound velocity are also discussed.

For the last ten years, studies on the physical properties of $5d$ transition metal oxides have revealed the importance of spin-orbit interaction (SOI).[1,2] In particular, in the case of Ir^{4+} ($5d^5$), the strong SOI splits the six-fold degenerate t_{2g} states into the occupied $J_{eff} = 3/2$ and half-occupied $J_{eff} = 1/2$ states.[1,3] The width of the bands

*E-mail address: p108090h@mail.kyutech.jp
†E-mail address: matuhira@elcs.kyutech.ac.jp

formed by the $J_{eff} = 1/2$ states is narrower than the width of the entire t_{2g} band in the absence of SOI. Consequently, the system can easily become a Mott-insulating state with even a moderate amount of correlations on the $5d$ electrons; the Mott-insulating state in Sr_2IrO_4 has been well studied as a typical case.[1,3] Recently, there has been a considerable increase in the research on Ir oxides because of their attractive physical properties, such as Kitaev spin liquid in A_2IrO_3, spontaneous Hall effect at zero field in $Pr_2Ir_2O_7$, metal-insulator transitions with all-in all-out ordering in $Ln_2Ir_2O_7$, and the prediction of a superconducting state owing to carrier doping for the SOI induced Mott-insulator Sr_2IrO_4.[4–11]

It is reported that SOI can affect phonon properties such as quantitative accuracy of phonon frequency, electron-phonon interaction, enhancement of spin-phonon coupling, and suppression of anharmonic potential.[12–20] In general, phonon dispersion is studied via inelastic neutron scattering and inelastic X-ray scattering (IXS) for single crystals. However, it is not easy to measure the phonon spectrum of iridium oxide using neutron scattering because Ir is a good neutron absorber; moreover, large single crystals are also required for this process. We can obtain the phonon dispersion of Ir oxide only via IXS measurements; IXS measurement as this process does not require large single crystals. On the contrary, IXS requires careful consideration because of the difficulty arising as a result of multiple scattering. Thus, direct observation of the phonon dispersion of the Ir oxides is quite limited[20] and is yet to be explored.

Recently, $Ca_5Ir_3O_{12}$ has been actively studied as a quasi-one-dimensional spin-orbit material. The crystal structure is a hexagonal structure with a space group of $P\overline{6}2m$ (No. 189),[21,22] and the primitive lattice includes three one-dimensional (1D) chains of the edge-sharing IrO_6; the three 1D rods form triangular lattices. The averaged valence of Ir ions is +4.67. $Ca_5Ir_3O_{12}$ exhibits semi-conductivity and has a two -phase transition.[21] One is an antiferromagnetic ordering below 7.8 K;[21,23,24] and the other is a second-order phase transition at 105 K, where the specific heat shows a sharp anomaly, and the electrical resistivity shows a sharp upward bend.[21,23,25] Presently, the origin of the phase transition at 105 K is not clear, because the structural and magnetic transitions for the powder samples have not been confirmed via XRD, neutron scattering, and μSR experiments.[21,24]

Our motivation is the need to clarify the origin of phase transition at 105 K. Recently, we performed Raman scattering measurement to understand the 105 K transition.[26] In this experiment, we observe superlattice instability. However, because Raman spec-

troscopy enables measurement of only the $\mathbf{q} = 0$ Raman active mode, it is difficult to extract specific characteristics of the phase transition. Therefore, the IXS measurement would be effective in the search for specific superlattice instability, because it can be accessible to the details of $\mathbf{q} \neq 0$ modes.

In this letter, we first show the results of phonon dispersion obtained via IXS measurements on the single crystals of $Ca_5Ir_3O_{12}$. The present study focuses on the room-temperature property, and results at low temperature are reported separately. To understand the experimental results, we have performed *ab initio* density-functional calculations for the phonon dispersion with the local density approximation (LDA) and the generalized gradient approximation (GGA) with SOI. We have then compared the calculated results with the experimental data, and found that the experimental phonon dispersion, Debye temperature, specific heat, and sound velocity are satisfactorily reproduced upon using the GGA calculation considering the SOI.

The IXS measurements were conducted at the BL35XU beamline of SPring-8 in Japan. We used two single crystals of $Ca_5Ir_3O_{12}$ crystals grown via the $CaCl_2$ flux method, as was previously reported.[25)] It was confirmed that these single crystals show the phase transition at 105 K in electrical resistivity measurements; these crystals are therefore of high quality. To measure the IXS in the c-plane and along the c-axis, these single crystals are attached to two types of sample holders, as shown in Fig. 1. We used both Si(11 11 11) and Si (9 9 9) backscattering optics, whose energy resolutions are ∼1.5 meV at 21.7 keV and ∼3 meV at 17.8 keV, respectively. The momentum resolution is (0.08, 0.03, 0.038) - (0.11, 0.04, 0.038) [r.l.u.] (depending on the direction) in the Si (9 9 9) setup, and (0.13, 0.10, 0.045) [r.l.u.] in the Si (11 11 11) setup. We measured Stokes and anti-Stokes components to correct the offset in energy transfer.

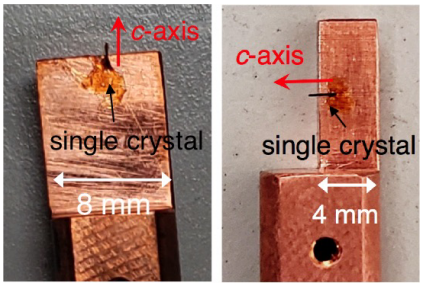

Fig. 1. (Color online) Sample holders used in these IXS experiments. Black and long thin single crystals are attached to a copper holder. The long direction of the single crystal corresponds to the c-axis (red arrow).

Figure 2 presents some examples of the fitting results of the IXS spectra. The IXS spectrum for the Stokes components measured at a fixed momentum transfer $\mathbf{Q}$ is given by

$$I(\mathbf{Q}, E) = I_e(\mathbf{Q}) + \chi(\mathbf{Q}, E)\frac{n(E)+1}{E} \tag{1}$$

where I_e is the elastic peak, E is the energy transfer, $\chi(\mathbf{Q}, E)$ is the scattering cross section of phonons, and $n(E)$ is the Bose factor.[27] $\chi(\mathbf{Q}, E)$ can be expressed as the sum of functions that have a peak at the energy of the phonon modes. The IXS data were analyzed using Eq. (1), where the elastic peak and phonon modes were fitted using an experimentally determined resolution function, which can in turn be fitted by a Voigt function. Following this, we demonstrate how to calculate the Voigt function corresponding to the resolution function. Because the Voigt function is calculated using the Faddeeva function $w(z)$ in this paper, the Voigt function is given by

$$V(E; \sigma, \gamma) = \frac{\mathrm{Re}[w(z)]}{\sigma\sqrt{2\pi}} \qquad \left(z = \frac{E + i\gamma}{\sigma\sqrt{2}}\right) \tag{2}$$

where σ and γ are the parameters of the Gaussian and the Lorentzian function, respectively.[28] Therefore, the full width at half maximum (FWHM) of the Gaussian (f_G), Lorentzian (f_L), and Voigt (f_V) functions are expressed in the following equations.[29]

$$\begin{aligned} f_G &= 2\sigma\sqrt{2\ln(2)} \\ f_L &= 2\gamma \\ f_V &= 0.5346 f_L + \sqrt{0.2166 f_L^2 + f_G^2} \end{aligned} \tag{3}$$

f_G and f_L are decided using the FWHM and the ratio of the Lorentzian and Gaussian functions of the resolution function. Therefore, the Voigt function corresponding to the resolution function can be calculated by substituting the σ and γ values obtained by fitting the resolution function into Eq. (2). Peak fitting is performed by multiplying the Voigt function by the intensity, and then adjusting the intensity as a parameter. As is shown in Figs. 2(a) and (b), the observed IXS spectra are well fitted by the fitting method described above, despite the resolution function difference depending on backscattering optics.

The Brillouin zone for $Ca_5Ir_3O_{12}$ is shown in Fig. 3(a). We measured the IXS spectra along the Γ-A, Γ-M, and Γ-K-M directions in the Brillouin zone, up to 60 meV; however, we could not obtain the IXS spectra above 40 meV with sufficient accuracy to assign the phonon mode because of the $1/E$ factor in Eq. (1). Figure 3(b) shows the IXS

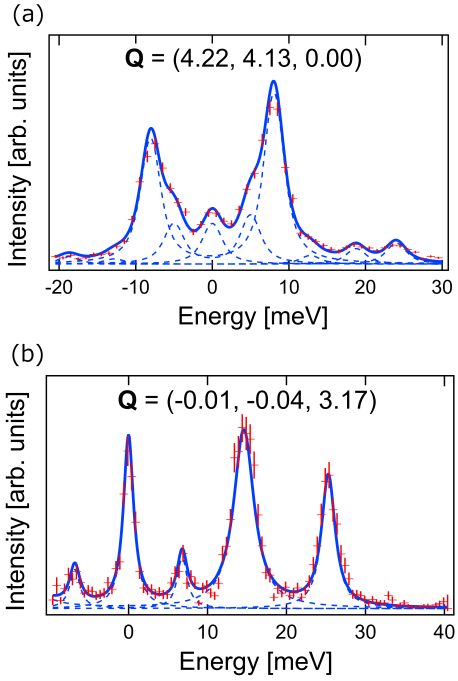

Fig. 2. (Color online) Fitting results of IXS spectra at room temperature for **Q** = (a) (4.22, 4.13, 0.00) and (b) (4.22, 4.13, 0.00). IXS data are shown by crosses with vertical error bars. The blue solid lines represent the fits summing up the Voigt peaks shown as dashed lines. The IXS spectra were measured in the (a) Si (9 9 9) and (b) Si (11 11 11) setup.

spectra below 40 meV with relative intensity color-coded on a logarithmic scale obtained for **Q** $\sim$ (4+q, 4+q, 0) (left), (8+q, 0, 0) (middle), and (0, 0, 3+q) (right) at room temperature. The phonon peak positions in Fig. 3(b) are determined using the Voigt fitting described above and are shown in Fig. 3(c) as closed symbols. To complete the dispersion where some phonon modes cannot be identified in Fig. 3(b), additional experiments were performed in different Brillouin zones; **Q** = (-q, q, 3), (-1+q, 1-q, 3), (-1-q, 1+q, 3), (4, 4, q), and (0, 9-q, 0) are shown as open squares, open triangles, open inverted triangles, open diamonds, and open circles in Fig. 3(c), respectively. To assign the observed phonon excitations, a calculation of phonon dispersion considering SOI is required.

Density functional calculations with plane-wave basis sets were performed using the xTAPP code,[30] in which we used the ultrasoft pseudopotential.[31,32] The LDA[33,34] and the GGA[35] were employed as the exchange-correlation potential. To study the effects of SOI, we performed the usual LDA and GGA calculations and compared them with the results, including the SOI. Below, we refer to the former as LDA (GGA) and to the latter as SO-LDA (SO-GGA). The cutoff energies in the wave function and

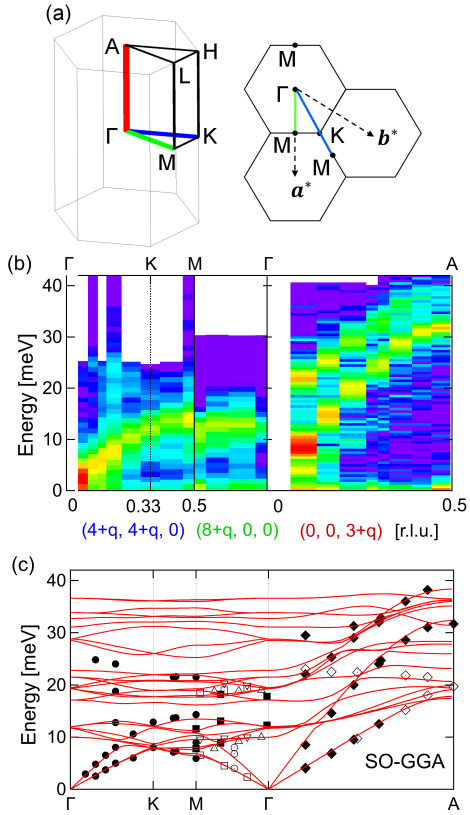

Fig. 3. (Color online) (a) The Brillouin zone of $Ca_5Ir_3O_{12}$. The figure on the left shows the first Brillouin zone. The figure on the right shows the Γ-K-M plane. Blue, green, and red lines are corresponding to the color of the horizontal axis label in Fig. 3(b). (b) IXS spectra with relative intensity color-coded on a logarithmic scale are, obtained for $\mathbf{Q} \sim (4+q, 4+q, 0)$ (left), $(8+q, 0, 0)$ (middle), and $(0, 0, 3+q)$ (right) at room temperature. (c) Comparison with peak positions from Fig. 3(b) (symbols) and calculations are obtained by GGA with SOI (SO-GGA) (red solid lines) in the reduced Brillouin zone. Additional peak positions obtained for $\mathbf{Q} \sim (-q, q, 3)$, $(-1+q, 1-q, 3)$, $(-1-q, 1+q, 3)$, $(4, 4, q)$, and $(0, 9-q, 0)$ are shown as open squares, open triangles, open inverted triangle, open diamonds, and open circles, respectively.

charge densities were 64 and 900 Ry, respectively. The atomic and lattice parameters were optimized with an $8 \times 8 \times 8$ k-point sampling. Phonon calculations with a frozen phonon approximation were performed using the PHONOPY package[36] for $1 \times 1 \times 3$ and $2 \times 2 \times 1$ supercells. For the k-point sampling, $11 \times 11 \times 11$ was used for $1 \times 1 \times 3$ supercell calculation, and somewhat coarse $9 \times 9 \times 5$ was used for the $2 \times 2 \times 1$ supercell calculation. In this paper, we show only the results of calculation for $1 \times 1 \times 3$ supercell. It was found that the experimental results at the room temperature are better reproduced by the $1 \times 1 \times 3$ supercell calculation.

Table I is a comparison between the theoretical and experimental crystal structures. For the lattice parameters a and c, the LDA values are smaller than the GGA ones, and this is a well- known trend.[37] With the SOI effect, the calculated parameters seem to increase slightly.[12] In comparison with the experimental values, the GGA and SO-GGA results have a rather good agreement, while the LDA and SO-LDA parameters are significantly underestimated from the experimental values.

Table I. Comparison between theoretical and experimental structural parameters of $Ca_5Ir_3O_{12}$. The experimental data with 120 K are taken from Ref. 21. The LDA (GGA) and SO-LDA (SO-GGA) indicate *ab initio* geometrical-optimization results based on local density approximation (generalized gradient approximation) without and with the SOI effect, respectively. The bottom row lists the Debye temperature Θ_D.

	LDA	SO-LDA	GGA	SO-GGA	Expt.
a [Å]	9.1283	9.1502	9.3631	9.3877	9.3490
c [Å]	3.1537	3.1541	3.2069	3.2118	3.1713
x_{Ca2}	0.7135	0.7129	0.7136	0.7129	0.7131
x_{Ir}	0.3336	0.3310	0.3315	0.3305	0.3334
x_{O1}	0.1986	0.1973	0.1992	0.1986	0.2008
x_{O2}	0.4598	0.4606	0.4590	0.4588	0.4620
x_{O3}	0.4477	0.4477	0.4458	0.4456	0.4559
y_{O3}	0.2466	0.2465	0.2440	0.2439	0.2407
Θ_D [K]	481.7	468.7	438.8	431.6	400

In Figs. 4(a) and (b) a comparison between the SO-GGA (thick -red curves) and SO-LDA (dashed -blue curves) phonon dispersions is illustrated. Panels (a) and (b) provide the phonon dispersion and density of the states, respectively. The SO-LDA phonon dispersion is prominently blue-shifted from the SO-GGA phonon dispersion, as already reported.[37] This blue shift trend is particularly appreciable in the high-frequency region near 50-90 meV, which reflects that the SO-LDA structure is more compact than the SO-GGA one, as shown in Table I. It should be noted here that SOI has an effect of increasing the lattice parameters slightly (see Table I). Therefore, SOI can bring about a small red shift in the phonon dispersion.

For a quantitative comparison with experiments in the low-frequency region, first, we compare in Fig. 4(c) the experimental specific heat (green dots) of $Ca_5Ir_3O_{12}$ in Ref. 21 with the calculation results by SO-GGA (red solid curves) and SO-LDA (blue dashed curves). We note that the two peaks in the experimental results correspond to the two phase transitions described in the introduction. The SO-GGA results are observed to have a better agreement with the experimental results than the SO-LDA results. We also estimated the Debye temperature Θ_D from the low-vibration phonon dispersion results. The results are is provided in the bottom row of Table I. The experimental value (400 K) estimated from the specific heat measurement is also shown,[21] from which we can observe that the SO-GGA (432 K) has the best agreement. There is a slight difference between the experimental and SO-GGA results in specific heat. This means that the experimental results are softer than those of SO-GGA.

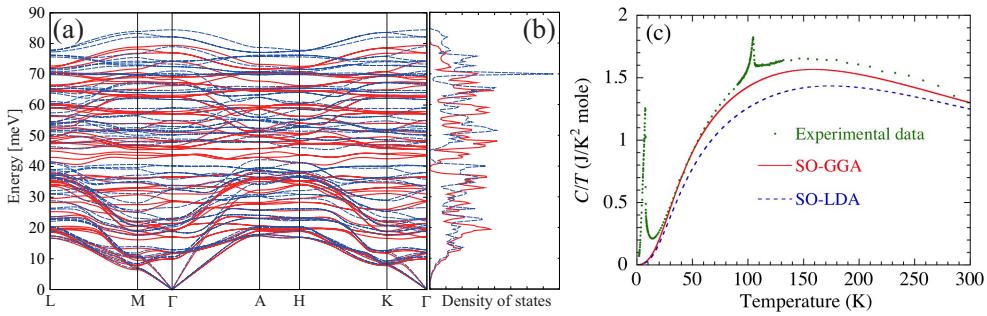

Fig. 4. (Color online) Calculated *ab initio* phonon dispersion (a) and density of states (b) of $Ca_5Ir_3O_{12}$. Thick red and dashed blue curves represent the SO-GGA and SO-LDA results, respectively. (c) Comparison of the experimental results (green point) for specific heat of $Ca_5Ir_3O_{12}$ in Ref. 21 with the calculation results by SO-GGA (thick red curve) and SO-LDA (blue dashed curve).

The experimental results of IXS are compared with the calculation results. The phonon dispersion obtained by SO-GGA is shown in Fig. 3(c). Because of the blue shift trend, as shown above, the SO-GGA dispersion results are closer to the experimental results than the SO-LDA results. The optical modes observed near 10-20 and 20-40 meV are the optical modes related to the Ir and Ca ions, respectively. All peak positions determined from the experimental data shown in Fig. 3(c) are assigned by the calculation obtained by SO-GGA; in particular, the observed acoustic phonon modes are in good agreement with the SO-GGA results. Next, we will also discuss the sound velocity (group velocities of acoustic phonon) that is obtained from the slopes of the longitudinal acoustic (LA) and transverse acoustic (TA) modes. Table II is a comparison

between the theoretical and experimental sound velocity of $Ca_5Ir_3O_{12}$. Experimentally, the slope of the LA and TA modes can be estimated from the peak positions around the Γ point in Fig. 3 (c). We can observe that the sound velocity along the *c*-axis is larger than that in the *c*-plane. From the comparison, we can conclude that the experimental results at room temperature are in good agreement with SO-GGA results.

Table II. Comparison between experimental and theoretical sound velocity v_s of $Ca_5Ir_3O_{12}$. v_s are obtained from the slope of longitudinal acoustic (LA) and transverse acoustic (TA) modes along Γ-K and Γ-A directions.

	Expt.	SO-GGA	SO-LDA
$v_s^{\Gamma-\mathrm{K,LA}}$ [km/s]	5.27 ±0.08	5.21	5.51
$v_s^{\Gamma-\mathrm{K,TA}}$ [km/s]	3.09 ±0.09	3.09	3.20
$v_s^{\Gamma-\mathrm{A,LA}}$ [km/s]	6.67 ±0.07	7.38	7.72
$v_s^{\Gamma-\mathrm{A,TA}}$ [km/s]	3.33 ±0.07	3.36	3.49

Thereafter, we mention the origin of the phase transition at 105 K. To this end, we performed a preliminary phonon calculation on a 2×2×1 supercell in addition to the 1×1×3 supercell. The former supercell includes the displacement degree of freedom in an in-plane 2×2 superlattice, and we can investigate the phonon instability within this superlattice. On the other hand, the latter 1×1×3 supercell can clarify the triple-period phonon instability along the *c*-axis. Within these two supercells, we did not observe phonon softening; there is no sign of softening at the A, K, and M points at room temperature. These results indicate that the phase transition at 105 K could be irrelevant to the structural phase transition with the **q** vector corresponding to at least the A, K, and M points. In the future, calculations for a large supercell including more displacement degrees of freedom and with stricter calculation condition would be desirable. From the experimental study, we need to reveal the temperature dependence of the phonon dispersion by IXS, which is an ongoing study.

In summary, this study demonstrated the phonon dispersion of iridium oxide $Ca_5Ir_3O_{12}$ at room temperature measured by IXS on the single crystals. In addition, we have provided the results of the calculation of phonon dispersion obtained by SO-

LDA and SO-GGA. The experimental phonon related properties, including the phonon dispersion, Debye temperature, specific heat, and sound velocity, have been compared with the calculation results, and are in a good agreement with the SO-GGA results. Regarding the phase transition at 105 K, no indication of phonon softening was obtained within the small size of the supercell, thus thereby requiring phonon calculations in larger supercells and stricter calculation conditions.

We thank M. Wakeshima for sharing specific heat data of $Ca_5Ir_3O_{12}$. The single crystal growth was supported by the ISSP Joint-Research program. The synchrotron radiation experiments were performed at the BL35XU of SPring-8 with the approval of the Japan Synchrotron Radiation Research Institute (JASRI) (Proposal Nos. 2018B1122, and 2019A1155). This work supported by grant of Kyushu Institute of Technology for research collaboration with other universities through utilization of research facilities, and the Promotion Project Uniting Strategic Program of the Kyushu Institute of Technology. This research was supported by JSPS KAKENHI Grant Number JP18H04327 (J-Physics). This research was partly supported by MEXT KAKENHI Grant Number JP15H03692. KN acknowledges supports by Grants-in-Aid for Scientific Research (No.16K05452, 16H06345, 17H03379, 17H03393) from MEXT, Japan.

References

1) B. J. Kim, Hosub Jin, S. J. Moon, J.-Y. Kim, B.-G. Park, C. S. Leem, Jaejun Yu, T. W. Noh, C. Kim, S.-J. Oh, J.-H. Park, V. Durairaj, G. Cao, and E. Rotenberg, Phys. Rev. Lett. **101**, 076402 (2008).

2) W. Witczak-Krempa, G. Chen, Y. B. Kim, and L. Balents, Annu. Rev. Condens. Matter Phys., **5**, 57, (2014).

3) B. J. Kim, H. Ohsumi, T. Komesu, S. Sakai, T. Morita, H. Takagi, T. Arima, Science, **323**, 1329 (2009).

4) A. Kitaev, Ann. Phys. **321** 2 (2006).

5) G. Jackeli and G. Khaliullin, Phys. Rev. Lett. **102**, 017205 (2009).

6) J. Chaloupka, G. Jackeli and G. Khaliullin, Phys. Rev. Lett. **105**, 027204 (2010).

7) Y. Machida, S. Nakatsuji, Y. Maeno, T. Tayama, T. Sakakibara, S. Onoda: Phys. Rev. Lett. **99**, 037203, (2007).

8) K. Matsuhira, M. Wakeshima, R. Nakanishi, T. Yamada, A. Nakamura, W. Kawano, S. Takagi and Y. Hinatsu: J. Phys. Soc. Jpn. **76** (2007) 043706.

9) K. Matsuhira, M. Wakeshima, Y. Hinatsu, and S. Takagi: J. Phys. Soc. Jpn. **80**, 094701 (2011).

10) F. Wang and T. Senthil, Phys. Rev. Lett. **106**, 136402 (2011).

11) Y.J. Yan, M. Q. Ren, H.C. Xu, B.P. Xie, R. Tao, H.Y. Choi, N. Lee, Y.J. Choi, T. Zhang, D.L. Feng, Phys. Rev. X **5**, 041018 (2015).

12) R. Heid, K.-P. Bohnen, I. Yu. Sklyadneva, and E. V. Chulkov, Phys. Rev. B **81**, 174527 (2010).

13) H. M. Tütüncü, H. Y. Uzunok, Ertuğru Karaca, and G. P. Srivastava, Phys. Rev. B **96**, 134514 (2017).

14) S. Calder, J. G. Vale, N. Bogdanov, C. Donnerer, M. Moretti Sala, X. Liu, M. H. Upton, D. Casa, Y. G. Shi, Y. Tsujimoto, K. Yamaura, J. P. Hill, J. van den Brink, D. F. McMorrow, and A.D. Christianson, Phys. Rev. B **95**, 020413 (2017).

15) C. H. Sohn, C. H. Kim, L. J. Sandilands, N. T. M. Hien, S. Y. Kim, H. J. Park, K. W. Kim, S. J. Moon, J. Yamaura, Z. Hiroi, and T. W. Noh, Phys. Rev. Lett. **118**, 117201 (2017).

16) H. Gretarsson, J. Sauceda, N. H. Sung, M. Höppner, M. Minola, B. J. Kim, B. Keimer, and M. Le Tacon, Phys. Rev. B, **96**, 115138 (2017).

17) J. Son, B. C. Park, C. H. Kim, H. Cho, S. Y. Kim, L. J. Sandilands, C. Sohn, J.-G. Park, S. J. Moon, and T. W. Noh, npj Quantum materials, **4**, 17 (2019).

18) W. Wang, J. Sun, and J. He, AIP Advances **9**, 025214 (2019).

19) K. Samanta, D. Rigitano, P. G. Pagliuso, and E. Granado, Appl. Phys. Lett. **114**, 152402 (2019).

20) C. D. Dashwood, H. Miao, J. G. Vale, D. Ishikawa, D. A. Prishchenko, V. V. Mazurenko, V. G. Mazurenko, R. S. Perry, G. Cao, A. de la Torre, F. Baumberger, A. Q. R. Baron, D. F. McMorrow, and M. P. M. Dean, Phys. Rev. B **100**, 085131 (2019).

21) M. Wakeshima, N. Taira, Y. Hinatsu, Y. Ishii, Solid State Commun., **125**, 311 (2003).

22) R.F. Sarkozy, W. Moeller, B.L. Chamberland, J. Solid State Chem. **9**, 242 (1974).

23) G. Cao, V. Durairaj, S. Chikara, S. Parkin, and P. Schlottmann, Phys Rev. B, **75**, 134402 (2007).

24) I. Franke, P.J. Baker, S.J. Blundell, T. Lancaster, W. Hayes, F.L. Pratt, G. Cao, Phys Rev. B, **83**, 094416 (2011).

25) K. Matsuhira, K. Nakamura, Y. Yasukuni, Y. Yoshimoto, D. Hirai, and Z. Hiroi, J. Phys. Soc. Jpn. **87**, 013703 (2018).

26) T. Hasegawa, W. Yoshida, K. Nakamura, N. Ogita, K. Matsuhira, J. Phys. Soc. Jpn. **89**, 054602 (2020).

27) Y. W. Cheung, Y. J. Hu, M. Imai, Y. Tanioku, H. Kanagawa, J. Murakawa, K. Moriyama, W. Zhang, K. T. Lai, K. Yoshimura, F. M. Grosche, K. Kaneko, S. Tsutsui, and Swee K. Goh, Phys. Rev. B **98**, 161103(R) (2018).

28) G. P. M. Poppe and C. M. J. Wijers, ACM Trans. Math. Software **16**, 38 (1990).

29) J.J. Olivero and R.L. Longbothum, J Quant Spectrosc. Radiat. Transf. **17**, 233 (1977).

30) J. Yamauchi, M. Tsukada, S. Watanabe, and O. Sugino, Phys. Rev. B **54**, 5586 (1996).

31) D. Vanderbilt, Phys. Rev. B **41**, 7892 (1990).

32) K. Laasonen, A. Pasquarello, R. Car, C. Lee, and D. Vanderbilt, Phys. Rev. B **47**, 10142 (1993).

33) D.M. Ceperley and B.J. Alder, Phys. Rev. Lett. **45**, 566 (1980).

34) J. Perdew and A. Zunger, Phys. Rev. B **23**, 5048 (1981).

35) J. P. Perdew, K. Burke, and M. Ernzerhof, Phys. Rev. Lett. **77**, 3865 (1996).

36) A. Togo and I. Tanaka, Scr. Mater. **108**, 1 (2015).

37) P. Haas, F. Tran, and P. Blaha, Phys. Rev. B **79**, 085104 (2009).